REPORT DOCUMENTATION PAGE

AFRL-SR-BL-TR-01-

0279

1. REPORT DATE (DD-MM-YYYY)	2. REPORT TYPE	3. DATES COVERED (From - To)
27-12-00	Final	01 May 98 - 30 April 00

4. TITLE AND SUBTITLE

Fundamental Studies of Model Electronic Devices Incorporating Self-Organized Quantum Dot Nanostructures

5a. CONTRACT NUMBER

5b. GRANT NUMBER

F49620-98-1-0460

5c. PROGRAM ELEMENT NUMBER

5d. PROJECT NUMBER

5e. TASK NUMBER

5f. WORK UNIT NUMBER

6. AUTHOR(S)

Lagally, Max G.

7. PERFORMING ORGANIZATION NAME(S) AND ADDRESS(ES)

University of Wisconsin-Madison
750 University Avenue
Madison, WI 53706

8. PERFORMING ORGANIZATION REPORT NUMBER

9. SPONSORING / MONITORING AGENCY NAME(S) AND ADDRESS(ES)

AFOSR/NE
801 N Randolph St Rm 732
Arlington VA 22203-1977

10. SPONSOR/MONITOR'S ACRONYM(S)

AFOSR/PK

11. SPONSOR/MONITOR'S REPORT NUMBER(S)

12. DISTRIBUTION / AVAILABILITY STATEMENT

Unclassified, Distribution unlimited

13. SUPPLEMENTARY NOTES

14. ABSTRACT

The objective of this research program was to perform fundamental studies to establish the utility of self-organizing Si/Ge nanostructures for eventual use in quantum-dot (QD) electronic devices. These studies consist of three major components: a) optimize the size and distribution of the three-dimensional pyramidal clusters that form in SiGe/Si(001) films and multilayers under defined growth conditions; b) design and simulate basic device building blocks and test structures for semiconductor devices that incorporate SiGe QDs, and c) make electronic and optoelectronic properties measurements and correlate these to structural and compositional ones to test the utility of arrays of pyramidal clusters for QD electronic devices.

15. SUBJECT TERMS

Silicon, germanium, quantum dots, growth, electronic properties

16. SECURITY CLASSIFICATION OF:			17. LIMITATION OF ABSTRACT	18. NUMBER OF PAGES	19a. NAME OF RESPONSIBLE PERSON
a. REPORT	b. ABSTRACT	c. THIS PAGE		22	M.G. Lagally
					19b. TELEPHONE NUMBER (include area code) 608-263-2078

Fundamental Studies of Model Electronic Devices Incorporating Self-Organized Quantum Dot Nanostructures

AFOSR Grant No. F49620-98-1-0460
Final Technical Report
01 May 98 - 30 April 00

Max G. Lagally
University of Wisconsin-Madison
Dept. of Materials Science and Engineering
Madison, WI 53706
Lagally@engr.wisc.edu
608/263-2078

Introduction and Objectives

The objective of this research program was to perform fundamental studies to establish the utility of self-organizing Si/Ge nanostructures for eventual use in quantum-dot (QD) electronic devices. These studies will consist of three major components: a) optimize the size and distribution of the three-dimensional pyramidal clusters that form in SiGe/Si(001) films and multilayers under defined growth conditions; b) design and simulate basic device building blocks and test structures for semiconductor devices that incorporate SiGe QDs, and c) make electronic and optoelectronic properties measurements and correlate these to structural and compositional ones to test the utility of arrays of pyramidal clusters for QD electronic devices. We use the simplest possible film structures that allow unequivocal determination of particular electronic properties and fabricate the structures that are essential to these studies.

Small pyramidal Ge or SiGe clusters grow in a self-organized fashion when Ge is deposited or Si and Ge are codeposited on Si(001). The strain induced by the lattice mismatch (4% maximum) causes the formation of these 3D islands, in accordance with the Stranski-Krastanov growth mode. Growing multilayers of alternately a film of SiGe alloy (forming these pyramidal clusters) and a film of Si (which acts as a spacer layer to embed the 3D pyramids) leads to further self-organization and the vertical replication of the quantum dots. However, none of the parameters required for good electronic properties – size, shape, spacing, composition, strain distribution – have been optimized. In fact, we do not even know what optimization means without making measurements to test the correlation between morphology and electronic properties. Our goal in this grant was to begin this process by choosing the simplest conditions for exploring electronic properties of SiGe QDs.

The grant includes a subcontract to RPI, Prof. Michael Shur.

Accomplishments/New Findings

a. QD growth optimization. We have learned how to vary sizes, shapes, and spacings of 3D QD islands in SiGe on Si(001) under a variety of growth conditions and to control these parameters with proper processing. We have been optimizing the processing parameters for the growth of these pyramid-shaped quantum dots in CVD and MBE as well as in a low-energy electron microscope (LEEM) outfitted with gas-source MBE. We have made progress in understanding how the pyramids can be made small in CVD and what needs to be done to maintain their shape when they are embedded in a Si matrix, as they always must be. Making them small is a matter of adjusting the composition and growing at low temperatures. We have learned to make them sparse or dense. We have learned what must be done to maintain shape during embedding.

We have also begun growth on laterally patterned substrates. We have learned in the LEEM how to make Si(001) mesas that are step-free over at least 10 micrometers. Growth on such substrates allows us to study in more detail the influence of defects on

the formation of 3D islands. Most recently we have begun to use silicon-on-insulator substrates for growth, and have also patterned these substrates. We have used Si template film thicknesses as low as 10nm.

Structural and morphological measurements we make routinely include AFM, TEM, and in-situ RHEED. RHEED is used to determine the onset of QD formation during growth in. TEM is used for cross-section studies of QD organization. AFM is used post-growth to observe QDs and QD arrays. STM is occasionally used in a parallel fashion to test particular ideas. Figure 1 shows several AFM images of different configurations of QDs grown on Si(001).

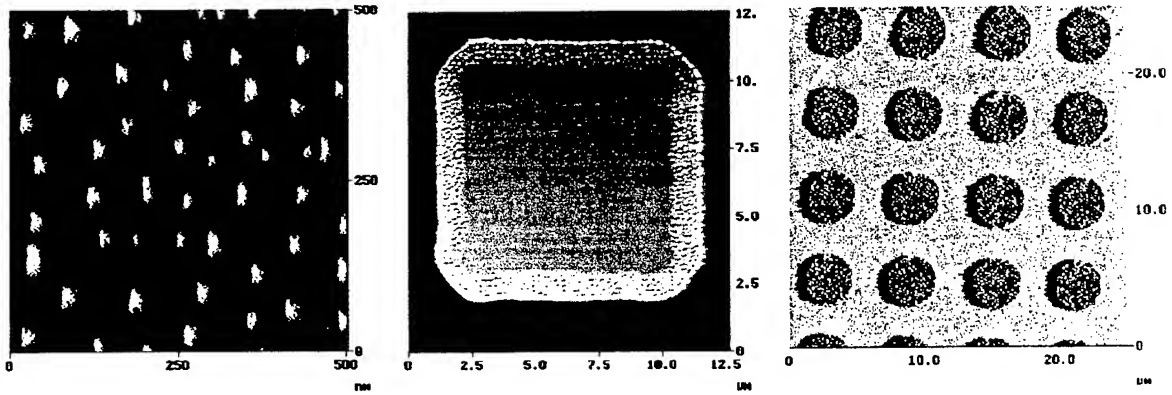

Figure 1: AFM images of quantum dots on Si(001). Left: Small and sparse pyramidal pure-Ge "hut" crystals; image taken with a carbon nanotube probe. These types of QDs (size and density) are used in the electrical measurements described later. Middle: a single step-free mesa of Si on SOI, about 10 microns square, with QDs. Most Ge nucleates at the edges to produce a window frame effect; some hut crystals are visible in the rest of the region. Right: a number of mesas on SOI, grown out so QDs fill the whole mesa.

b. Review of band structures of Si and Ge and effect of strain. Figure 2 shows schematically the band structures of bulk Si and bulk Ge. Both are indirect-gap materials. For Si, the conductance band minimum is at the X point, and is 6-fold

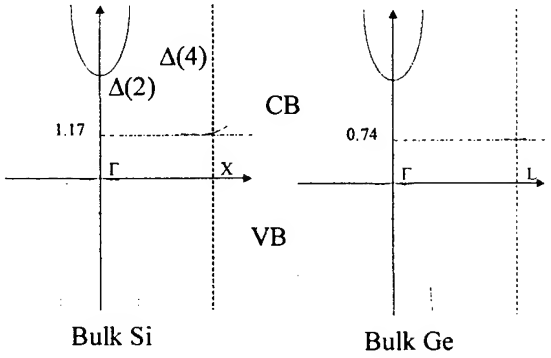

Figure 2: Schematic band diagrams of bulk Si and Ge.

degenerate ($\Delta(2) + \Delta(4)$). For Ge, the conductance band minimum is at the L point and it is 4 fold degenerate. At 0K, the gaps between minima of the conductance band to the maxima of the valence band are 1.17eV and 0.74eV for Si and Ge respectively. Strain affects this band structure. For heteroepitaxy, a biaxial strain is induced, which resolves into a hydrostatic strain and a uniaxial strain, as shown in Fig. 3. The hydrostatic strain shift both the positions of conductance band and valence band while the uniaxial strain splits the conductance band from 6-fold degeneracy to two minima [$\Delta(2)$ and $\Delta(4)$] and the valence band to two levels [heavy hole and light hole]. If the strain is compressive, as it is in epitaxially grown Ge on Si, the conductance band minimum is at $\Delta(4)$, while the valence band maximum is at the heavy-hole maximum.

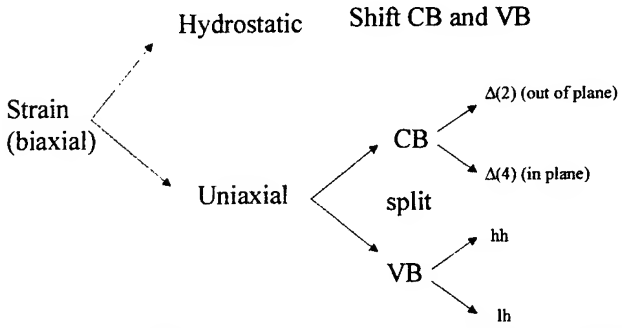

Figure 3: Effect of strain on band structure in SiGe.

Figure 4 shows the band structure of SiGe alloy grown on Si. The dotted lines are the conductance and valence band energies of unstrained SiGe. The conductance and valence bands split as the Ge content increases. For pure Ge on Si, the strained band gap is only about 0.5eV between $\Delta(4)$ and the heavy-hole band maximum. The valence band offset for strained Ge on Si is about 0.7eV. The conductance band offset is relatively small. It is about 0.05eV.

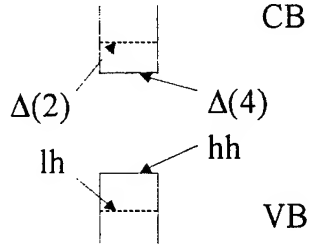

Δ(2): CB out of plane (2-fold)

Δ(4): CB in plane (4-fold)

lh: light hole

hh: heavy hole

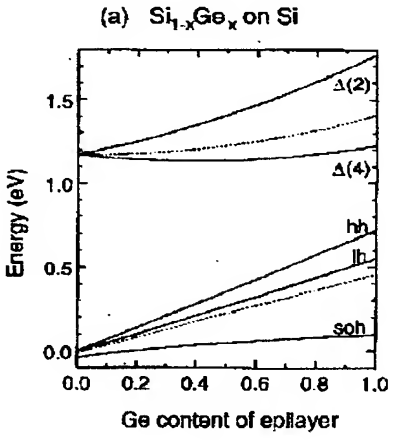

Figure 4: Dependence of band edges on Ge concentration in Si.

c. Review of quantum confinement. Quantum dots with diameter smaller than 100nm can be viewed as artificial atoms with discrete energy levels and s-p like orbital occupation of electrons or holes. A simple parabolic lateral potential can be used to describe the quantum confinement in quantum dots. The height of the potential barrier is from the ground state energy to the Si valence band edge. The ground state energy is mainly determined by the vertical confinement of the quantum dots, which is usually much larger than the lateral confinement. (For Ge dots with {105} facets, the vertical size is about 10 times smaller than it base size). By this approximation, the heavy-hole state separation is $E_N = (N + \frac{1}{2})\hbar\omega$, with

$$\omega = \sqrt{\frac{k}{m^*_{hh}}} = \frac{2}{D}\sqrt{\frac{2(E_{ground} - E_v)}{m^*_{hh}}} \quad .$$

D is the average diameter of the quantum dots, and E_v and E_{ground} are Si valence band energy and ground state of Ge quantum dots respectively. For a quantum dot with size D~30nm, the ground state energy with respect to the Si valence band edge measured with PL (see below) is ~330meV. The heavy-hole separation energy E_N is then about 28meV.

In addition, the self-capacitance of a small quantum dot is on the order of 10^{-17}-10^{-18} F. Therefore, Coulomb-charging effects cannot be neglected. Charges inside a quantum dot are very close to each other, hence the Coulomb repulsion is large enough to cause a large change of holes separation energies solely due to the quantum confinement effect. For a quantum dot with size D~30nm, the energy gain due to Coulomb charging $\Delta E_{coulomb}$ is about 12meV, comparable with the heavy hole separation energy.

d. Design basic electronic-device building blocks. Our approach has been to look at film structures with one or more buried QD layers for potential electronic/optoelectronic devices, rather than thinking about devices that would make use of a single quantum dot. Our intent has been to make device structures that will allow us to test the electronic properties that result from variations in the properties of a QD layer (or layers). We are interested in exploring the following properties:

- Are holes trapped in the QD layer?
- Can we estimate the number of holes trapped on average in a QD?
- Can we determine the thermal activation energy of heavy holes in QDs?
- Can we determine the ground state energy of heavy holes?

We have prepared device structures that allow us to measure these properties. Figure 5 shows a schematic diagram of one to these structures along with an AFM image of the size and density of QDs that were in this layer. After the QD layer is buried, the QD size may change slightly and the composition will become less Ge rich, but the dot density remains the same. The structures have a front Schottky contact to enable band bending and an ohmic contact on the back.

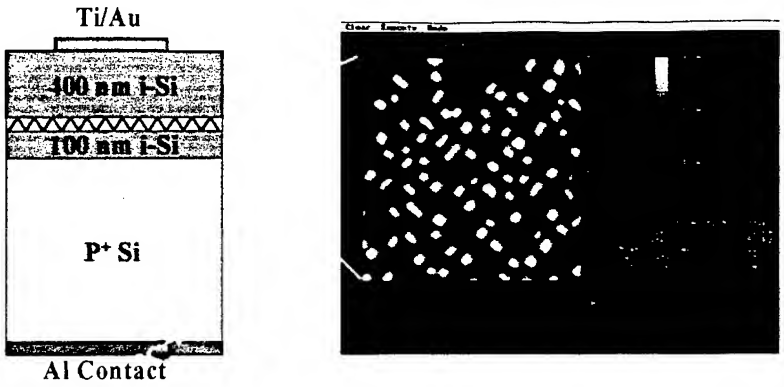

Figure 5: Simple device structure containing one layer of Ge QDs, along with AFM image of these dots before they are buried by the top Si layer. The sample is grown by s MBE with substrate temperature 550°C. A P^+ substrate with resistivity 0.001-0.002 Ωcm ($\sim 10^{19} cm^{-3}$ doping level) is used. 100 nm thick undoped Si is grown as a buffer layer. After that, 6 ML of Ge is deposited. Then the sample is capped with 400 nm undoped Si. Note the QD density and size.

e. Electrical measurements. The following types of measurements were made:

Electrical:

Multi-frequency C-V: determine whether holes are trapped in the QD layer and estimate the number of holes trapped per dot

Admittance spectroscopy: Thermal activation energy of heavy holes in dots

Figure 6 shows schematically the experimental setup for the electrical measurements.

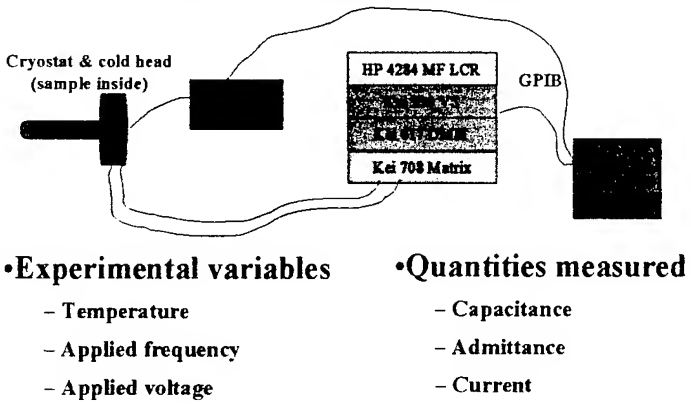

Figure 6: Experimental setup for electrical measurements.

We have made C-V measurements on samples such as that shown in Fig. 5, both with a single layer of QDs and with two layers of QDs. From the C-V measurements we can, by

differentiation, determine the holes trapped in the QD layer, and from the QD density determined with AFM, we can extract the average number of holes in a QD. Our results give **6 holes per QD!** The results are illustrated in Fig. 7.

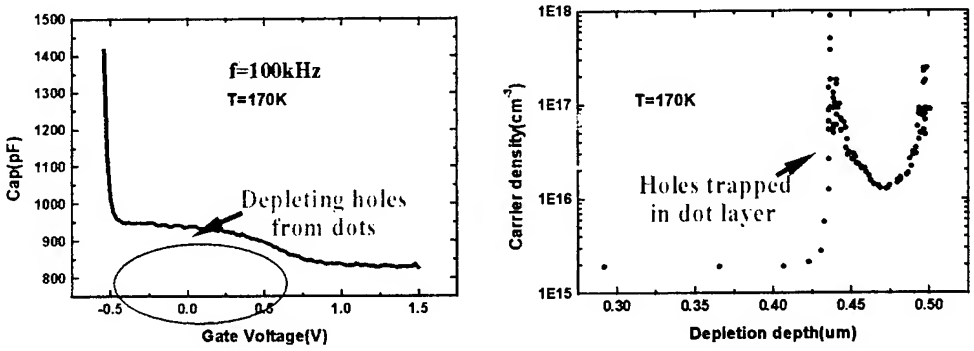

$$\#\,holes/dot = \frac{\int_{depletion} CdV}{eN} \qquad n(V) = \left(\frac{2}{q\varepsilon\varepsilon_0}\right)\left(\frac{d(1/C^2)}{dV}\right)^{-1}$$

***N*: # of dots under test**

6 holes per dot!!

Figure 7: C-V measurement of the sample shown in Fig. 5 at 170K and 100kHz. An accumulation of charge in the QD layer is clearly evident. The carrier density profile is shown in the right panel. Analogous measurements as a function of temperature show a decrease in the width of the plateau region in the C-V measurement. At temperatures below 85K, there is no plateau at all, indicating that no carriers inside the QD layer contribute to the capacitance reading. Below this temperature the carriers cannot respond to the rapidly changing external signal. The carriers are frozen inside the QD layer. Because in C-V the differential capacitance is being measured, by integrating the capacitance in the voltage range where charges are depleted from the Ge QD layer, the total charge being depleted from the QD region can be obtained. Dividing the total charge by the number of QDs under the contact area yields the average number of charges being stored inside one QD. This integration gives about 6 holes per dots.

Admittance spectroscopy at different temperatures was performed to obtain the thermal activation energies of holes inside the QDs. There are usually several energy levels due to quantum confinement. By applying an external DC voltage, the Fermi level can be changed relative to these quantum levels. Only holes with energy nearest to the Fermi level will be depleted from the quantum dots. In this way, different energy levels can be approached.

The experiment is done at temperatures from 100K to 295K with 5K steps. The temperature resolution is better than 0.5K. At each temperature point, capacitance and conductance are measured at frequencies of 50k, 80k, 100k, 200k, 400k, 600k, 800k and 1MHz with applied gate bias from 0V to 2V with 0.2V steps. Figure 8 shows results.

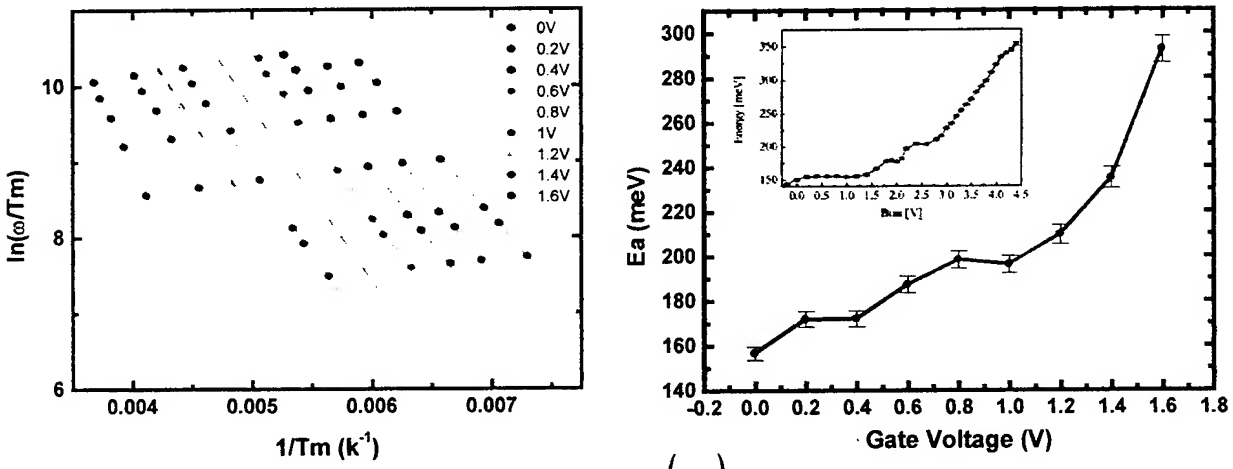

$$E_a = k_B \frac{d \ln\left(\frac{\omega}{T_m}\right)}{d\left(\frac{1}{T_m}\right)}$$

Figure 8: Results of admittance spectroscopy of a single QD layer in the structure shown in Fig 5. Left panel: Arrhenius plots from admittance spectroscopy at various bias voltages. The slopes of these curves give the activation energy of holes at different biases. Activation energies range from 155meV to 295meV as a function of bias voltage, plotted in the right panel. It is likely that in these experiments the QD density of states is quasi-continuous, because of the breath of each level caused by the size distribution in the ~10^{10} QDs participating in this measurement. Inset: Result by Absreiter for much larger QDs containing about 70 holes per dot.

f. Optical measurements. Photoluminescence measurements were made to obtain the ground state energy of heavy holes in the QDs. Some results are shown in Fig. 9. From them we can determine the ground state energy of the holes. The PL from quantum dots is regarded as a spatially type II transition. The recombination occurs between holes at the ground state and the Si conductance band edge. Assuming that the QD transition is a non-phonon assisted transition, then the position of the QD peak gives the ground state energy of the holes. In this case, the ground state is about 330meV. The FWHM is about 90meV, representing the size distribution of the quantum dots.

Our results suggest that a tuneable wavelength QD infrared photodetector can be fabricated from SiGe QDs. A possible structure is shown in Fig. 10. A multilayer structure of doped QDs are grown in the manner that we have developed. The size distribution be-

comes narrower as more layers are added. The device is tuned by tuning the vertical gate voltage.

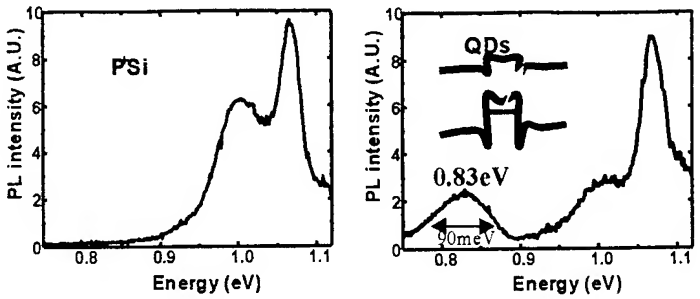

Spatially type II transition
From ground state to Si CB edge ~330meV
FWHM ~90meV (size distribution)

Figure 9: PL spectra, taken at 12K of Si substrate and the structure shown in Fig. 3, containing the QD layer. The separation of the QD peak at 0.83eV and the Si peak is 330meV. The width of the QD peak is due to the size distribution of the QDs in the field of view of the laser beam.

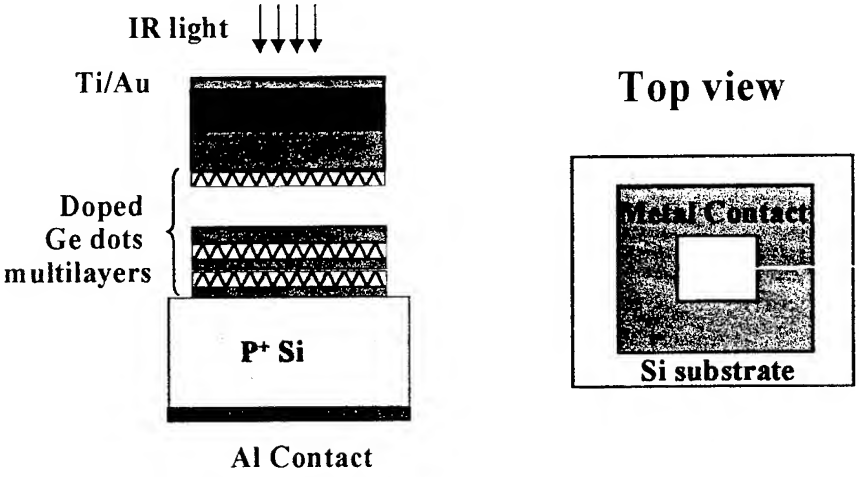

Absorption wavelength is tuned by vertical gate voltage

Figure 10: Schematic diagram of a wavelength tuneable QD IR photodetector. The viability of this QDIP is demonstrated by our results.

Summary

We have grown self-assembled SiGe QD films and multilayers and have characterized growth with a view toward making structures that are most suitable for QD electronic devices that use an ensemble of QDs rather than just one.

We have made simple device structures from these films. We have developed processing conditions suitable for making device structures that contain QD layers, which are sensitive to high-temperature processing.

From electrical measurements we determined:

An average of 6 holes per QD
Activation energies of heavy holes in QDs
Quasi-continuous density of state due to size distribution of QDs.

From PL measurements we determined:

Heavy hole ground state energy is 330meV

Our results suggest a potential application of QD multilayers for tunable-wavelength IR detectors.

Personnel directly supported on this grant

Frank Flack
Yuegang Zhao
Feng Liu
Paul Rugheimer
Todd Narkis
Mark Friesen
Max G. Lagally

Publications

The following were partially supported by this grant:

"Spontaneous Self-Embedding of Three-Dimensional SiGe Islands", E. Mateeva, P. Sutter, and M.G. Lagally, Appl. Phys. Letters 74, 567 (1999).

"Properties of $Si_{1-x}Ge_x$ Three-Dimensional Islands," J.S. Sullivan, E. Mateeva, H. Evans, D.E. Savage, and M.G. Lagally, J. Vac. Sci. Technol. A17, 2345 (1999).

"Mechanisms Determining Three-Dimensional SiGe Island Density on Si(001)", J. S. Sullivan, H. Evans, D.E. Savage, M.R. Wilson, and M.G. Lagally, J. Elect. Mat. 28, 426 (1999).

"Dislocation-Induced Surface Strain on (001) Silicon-On-Insulator", P. Sutter and M.G. Lagally, Epitaxial Growth - Principles and Applications, eds. A.-L. Barabasi, M. Krishnamurthy, Feng Liu, and T. Pearsall, MRS Proceedings 570, 235 (1999).

"Strain Engineering of Nanoscale Structures in the Ge/Si System", Feng Liu and M. G. Lagally, in Precision Science and Technology for Perfect Surfaces, eds. Y. Furu-

kawa, Y. Mori, and T. Kataoka, Proceedings of the 9th International Conference on Production Engineering (ICPE9), Publication Series No. 3, Japan Society for Precision Engineering, Tokyo, Japan, 1999, pg. 648.

"Strain, Morphology, and Self-Organization in the Growth of Si/Ge 'Quantum Dot' Nanoclusters", A.R. Woll, J. S. Sullivan, Feng Liu, and M. G. Lagally, in Cluster and Nanostructure Interfaces, eds. P. Jena, S.N. Khanna, and B.K. Rao. World Scientific, 2000, pg 631.

"Electrical and Optical Characterization of SiGe Quantum Dots in Si(001)", Y. Zhao, F. Flack, P. Rugheimer, M. Erikkson, and M.G. Lagally, in preparation.

"Self-Organized Quantum Dots", P.P. Rugheimer, A. R. Woll, and M.G. Lagally, Int. J. High-Speed Electronics and Systems, in preparation.

Interactions/Transitions

a. presentations

Oral presentations were made at annual APS and MRS meetings, primarily describing the QD growth results.

b. consultative and advisory functions

None

c. transitions

None

New discoveries

Demonstration that holes are trapped in SiGe QDs and that we could determine their number - average of 6 per QD.

Activation energies of holes in QD.

Potential tuneable QD IR photodetector.

Honors/Awards

Max Lagally was elected to Leopoldina, the German National Academy of Sciences, in 1999. He was also elected a Fellow of AAAS, in 2000, somewhat after the end of the grant period.

Jeff Sullivan received a Materials Research Society Graduate Student Award and the American Vacuum Society Nanoscale Sciences Best Paper Award.

Subcontract

This grant included a subcontract to Prof. Michael Shur at RPI, primarily for theoretical studies. The work at RPI was highly successful. Because of the initially rather slow rate of the experimental work, there was less collaboration and overlap between the two efforts than we would have liked. Much potential exists at this stage for such further collaboration, given the status of the experimental work at present.

Executive Summary

We showed that the space dependence of the effective mass in quantum wires results in appearance of additional momentum-dependent potential. If the effective mass is anisotropic (as in silicon or germanium), this effect strongly depends on the transverse mass for a given subband. We considered Si-Ge p-type quantum wires, where the impact ionization by holes should be determined by the impact ionization rates in silicon, and not in SiGe.

We also proposed a semi-analytical model for the quantum dots spectra that accounts for the space dependence of electron (hole) effective mass and the effective mass anisotropy of the dot material and of the surrounding matrix. This dependence and this anisotropy significantly affect the position of the quantum levels. Our analysis shows that quantum dot spectra are relatively insensitive to the exact shape of the quantum dots.

The results of this work have been published in two refereed publications and will be included into the book on quantum dots that we are now editing (see Section 4 of the Report).

1. Consequences of space dependence of effective mass in quantum wires

Introduction

The space dependence of the effective mass in quantum wires results in appearance of additional momentum-dependent potential. If the effective mass is anisotropic (as in silicon or germanium), this effect strongly depends on the transverse mass for a given subband. As an example, we considered Si-Ge p-type quantum wires, where the impact ionization by holes should be determined by the impact ionization rates in silicon, and not in SiGe.

In the heterostructure devices with quantum wells, quantum wires or quantum dots, the electron effective mass depends on coordinate. Several authors (see, for example, [1-3]) considered the consequences of the space dependence of electron effective mass for quantum wells of finite depth formed by two materials with parabolic conduction bands and different electron masses in the barrier and well region.

As shown in [1-3], the space dependence of effective mass leads to the appearance of momentum-dependent additional potential, $U(q)$

$$U(q) = q^2(\frac{1}{2m_1} - \frac{1}{2m_2}), \tag{1}$$

where m_1 and m_2 are the effective masses in the quantum well and barrier regions, respectively (see Fig.1a), and q is the longitudinal momentum. As can be expected from the Kane model, the electron effective mass in the narrow band material is usually smaller than in the wide-band material $(m_1<m_2)$. Hence, the additional potential $U(q)$ leads to the disappearance of quantum well for the electrons (or holes) with the longitudinal momentum

$$q^2 > q_{cr}^2 = \frac{U_0}{(1/2m_1 - 1/2m_2)} \tag{2}$$

Here U_0 is the depth of the potential well created by the conduction (or valence) band discontinuities. As predicted in [3], the electrons (or holes) with such q's are localized in the barrier region of the heterostructure.

In the simplest case of quantum wire formed by two materials with parabolic conduction bands, the total energy is given by

$$E = \frac{p_x^2}{2m_x} + \frac{p_y^2}{2m_y} + \frac{q^2}{2m_z} + U(x,y), \tag{3}$$

where p_x and p_y are the size-quantized components of the momentum in the x-y plane, perpendicular to the wire axis, q is the longitudinal component of the momentum in the wire direction, m_x, m_y are the effective masses for the motion in the x and y directions, respectively, and $U(x,y)$ is the electron potential energy. In Eq.(3),
$U_q(x,y) = q^2 / 2m_z(x,y)$ is the additional momentum dependent potential, so that the total effective potential is given by

$$U_{eff}(x,y) = U(x,y) + U_q(x,y). \tag{4}$$

If $m_z(x,y)$ is constant and independent of the motion direction, the effective potential differs from the real potential by a constant. However, if the effective mass depends on the coordinates, the effective potential depends on the longitudinal momentum q.

The energy level in the quantum wire of depth U_o differs from the energy level in the quantum well of the same depth. The energy level in the wire is closer to the top of the potential well, and, in the case of a very shallow potential well, the level energy is exponentially small in comparison to the potential depth.

On the other hand, the common feature of one- and two-dimensional confinement is the existence of an energy level in the potential of an arbitrary depth. Therefore, the condition of the disappearance of the confinement potential is the same for a quantum wire as for a quantum well, see Eq. (2). However, the dependence of the energy level position on q in the quantum wire is different from that for a quantum well.

For a quantum well, the anisotropy of effective masses leads to the following equation for the critical longitudinal momentum:

$$U_0 = q_y^2(\frac{1}{2m_{y1}} - \frac{1}{2m_{y2}}) + q_z^2(\frac{1}{2m_{z1}} - \frac{1}{2m_{z2}}).$$

For a quantum wire, the critical value of the longitudinal momentum is given by

$$q_{cr}^2 = \frac{U_0}{\frac{1}{2m_{z1}} - \frac{1}{2m_{z2}}} \tag{5}$$

Hence, the influence of anisotropy of the effective mass in quantum wire on the critical value of longitudinal momentum is strongly dependent on the transverse effective mass corresponding to a given subband, i.e. this value is different for levels corresponding to $m_z = m_\perp$ and $m_z = m_{||}$. We consider the influence of anisotropy using a Si-Ge quantum wire as an example.

Rectangular Quantum Wire

The dependence of potential for the transverse motion $U_{eff}(x,y)$ on the longitudinal momentum q leads to the dependence of the size-quantized energy on q. Hence, the position of the quantum level of localized electrons with different q depends on q, and the energy spectrum is nonparabolic.

We consider the rectangular quantum wire of finite depth U_o. Practical quantum wires do not usually have a rectangular cross-section. However, the position of energy level in quantum wire of a finite depth only weakly depends on the shape of cross-section (see Ref.4). The comparison of our results for rectangular wires with our own calculations for the quantum wires with circular cross-section, confirm the conclusion reached in Ref.4. The potential depth of the quantum wire strongly depends on strain, however the effect of strain could be accounted for the renormalization of potential depth U_o [5,6].

The calculation of the spectrum for the case of rectangular quantum wire yields the following expression for the electron energy, E:

$$E = -U_0 + \frac{2\hbar^2}{m_{x1}a^2}\left(k_x^2 + \frac{m_{x1}}{m_{y1}}k_y^2 + \frac{m_{x1}}{m_{z1}}\eta^2\right)$$

Here U_0 is the potential wire depth, a is the size of the wire in x direction, $\eta = qa/2$ is dimensionless longitudinal momentum. The dimensionless components of transverse momentum k_x and k_y are the solutions of the following system of equations

$$\frac{k_x}{\sqrt{k_x^2 + \delta^2}} = \cos\frac{k_x}{2}$$

$$\frac{k_y}{\sqrt{k_y^2 + \delta^2 \frac{m_{x1}}{m_{y1}}\frac{m_{y2}}{m_{x2}}}} = \cos\frac{k_y\beta}{2\sqrt{m_{x1}/m_{y1}}}. \tag{6}$$

Here $\beta = b/a$ is the size ratio of the wire in the x and y directions,

$$\delta^2 = \left(\frac{m_{x2}}{m_{z2}} - \frac{m_{x2}}{m_{z1}}\right)\eta^2 + \frac{\chi - k_x^2 + \frac{m_{x1}}{m_{y1}}k_y^2}{\alpha},$$

$$\chi = \frac{2U_0 m_{x1}}{\hbar^2},$$

$$\alpha = m_{x1}/m_{x2}.$$

Equations (6) describe all energy states even with respect to x and y, including the lowest energy level. For the levels corresponding to the odd states, the right-hand sides of equations (6) are to be replaced by $\sin(k_x/2)(\sin(k_y\beta\frac{m_{y1}^{1/2}}{2m_{x1}^{1/2}}))$.

For isotropic and equal effective masses (α=1), we obtain the standard solution describing a two-dimensional confinement, and the $E(q)$ dependence is parabolic.

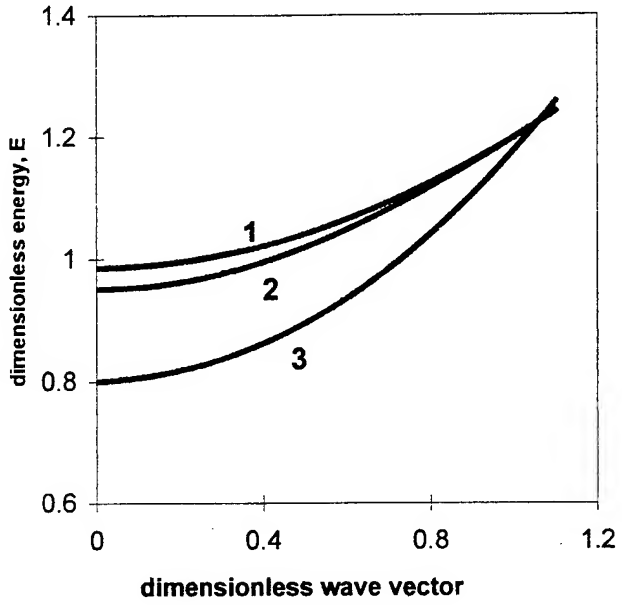

Fig.1. Dimensionless energy, E, versus η for α=0.2,χ=1. Lines: 1 - β=1, 2 - β=10, 3 – quantum well.

For an isotropic but space dependent effective mass (and $\alpha < 1$), the bound states disappear for $q^2 > q_{cr}^2 = \chi/(1-\alpha)$. Fig. 1 shows the energy spectrum for the lowest subband for $\chi=1$, $\alpha=0.2$. For these parameter values, there is only one energy level. Curve 1 corresponds to the square quantum wire ($a = b$), curve 2 corresponds to the case b/a=10, and curve 3 corresponds to the quantum well of the same depth. The positions of levels are different for $q<q_{cr}$, but for $q = q_{cr}$ all curves converge at the same point, since the energy level exists for the one- and two-dimensional confinement for an arbitrary potential depth, not matter how shallow. At $q = q_{cr}$, all spectra terminate. The dispersion relation for the isotropic but space dependent effective mass in the quantum wire was considered also in Ref. 7. For this case, their results agree with ours.

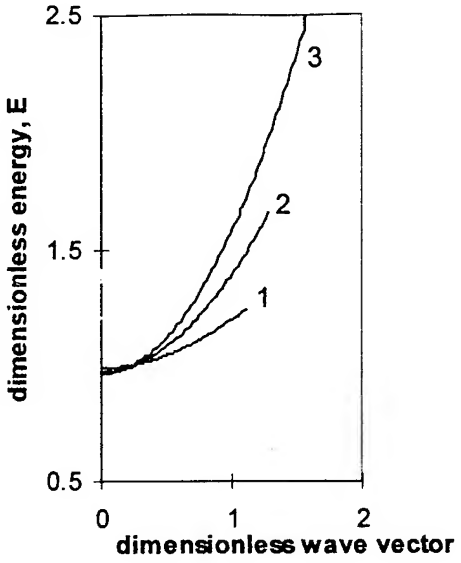

Fig.2 Dimensionless energy, E versus η for different α and χ=1. Lines: 1 - α=0.2, 2 - α=0.4, 3 - α=0.6.

Fig. 2 shows the dependence of energy E versus η for different values of α for a square quantum wire with dimensionless potential depth χ=1. As can be seen from the figure, q_{cr} decreases with the decrease of α.

The influence of anisotropy of the effective mass depends on the mass in the direction of quantization corresponding to a given quantum level . If the level corresponds to the value of effective mass $m_x = m_z = m_\perp$, $m_y = m_\parallel$ (type *a* level) the critical value of longitudinal momentum is given by Eq. (5), where m_{z1} and m_{z2} have to be replaced with $m_{\perp 1}$ and $m_{\perp 2}$ respectively.

If the quantum level corresponds to the effective mass $m_x = m_y = m_\perp$, $m_z = m_\parallel$ (type b level) masses m_{z1} and m_{z2} in Eq. (5) have to be replaced with $m_{\parallel 1}$ and $m_{\parallel 2}$ respectively. Fig.3 shows a dependence of the energy (E) on η for levels of types (a) and (b) for α=0.2, $m_{\perp 1}/m_{\parallel 1}$=0.2, $m_{\perp 2}=m_{\parallel 2}$.

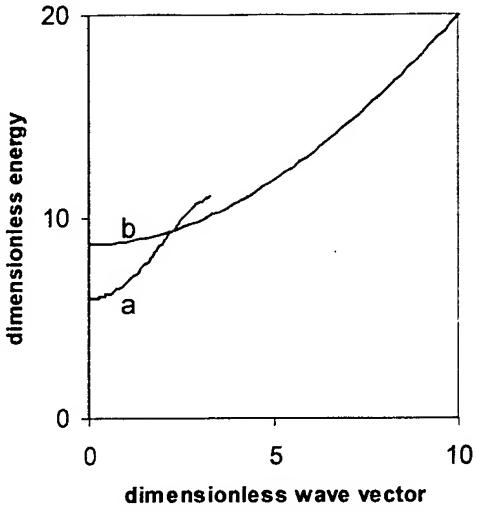

Fig.3 Dimensionless energy, E versus η for χ=10, β=1. α=0.2, $m_{\perp 1}/m_{\|1}$=0.2, $m_{\perp 2}/m_{\|2}$=1. Lines (a) and (b) correspond to the levels of type (a) and (b).

The SiGe Quantum Wire

As an example, we consider a p-type SiGe wire with 30% Ge molar fraction. In this case, the heavy hole masses are isotropic and weakly nonparabolic [6]. The effect of strain can be taken into account by the renormalization of potential depth of quantum wire [6]. We can apply to this case the same theory as for electrons. For the Ge rectangular quantum wire with 7nm*7 nm cross-section, the 2D spectrum terminates at 280 meV. Hence, the impact ionization by holes in the Si-Ge quantum wired will be determined by the impact ionization rates in silicon, and not in SiGe. This result is similar to that for electrons in AlGaN/GaN/AlGaN quantum wells [3]. In the same way, the effects of the real space transfer [2] of holes from the quantum wires into the cladding layer as well should be affected.

2. Consequences of space dependence of effective mass in quantum dots

Introduction

We propose a semi-analytical model for the quantum dots spectra that accounts for the space dependence of electron (hole) effective mass and the effective mass anisotropy of the dot material and of the surrounding matrix. This dependence and this anisotropy significantly affect the position of the quantum levels. Our analysis shows that quantum dot spectra are relatively insensitive to the exact shape of the quantum dots.

The common feature of one- and two-dimensional confinement is the existence of an energy level in the potential of an arbitrary depth. Therefore, the condition of disap-

pearance of the confinement potential is the same for a quantum wire as for the quantum well. The difference between one- and two-dimensional confinements is reflected only in the energy level positions.

The situation for the case of quantum dot differs from that for quantum wells and wires. In a shallow quantum dot, the quantum level doesn't exist. The level appears if the potential depth exceeds

$$U_{0\min} = \frac{\pi^2 \hbar^2}{8ma^2}, \qquad (7)$$

where a is the linear size of the dot, and m is the mass of the particle in the dot [8]. In this article, we discuss the electronic (holes) states in quantum dots with varying effective mass. We take into account the effective mass anisotropy, and compare our results with the results of the numerical calculations for InAs quantum dots [4].

In the simplest case of quantum dot formed by two materials with parabolic conduction bands, the total energy is given by

$$E = \frac{\hbar^2 k^2}{2m_1} + U_0,$$

where k is the size-quantized component of the wave vector. For a spherical quantum dot, the value of k is found by solving the following algebraic equation

$$ctg(ka) = \frac{ak}{\sqrt{\alpha(\frac{2m_1 a^2 U_0}{\hbar^2} - a^2 k^2)}}. \qquad (8)$$

Here $\alpha = m_1 / m_2$. Eq. (8) shows that the space dependence of effective masses of electron (hole) doesn't change the critical potential of the appearance of the energy level in quantum dot, i.e. the energy level appears if the potential depth exceeds the value given by Eq.(7) with $m = m_1$. However, the energy level positions for electrons (or holes) in a quantum dot strongly depends on α.

Rectangular Quantum Dot.

The calculation of the spectrum of the case of rectangular quantum dot yields the following expression for the electron (hole) energy, E:

$$E = -U_0 + \frac{2\hbar^2}{m_{x1} a^2}(k_x^2 + \frac{m_{x1}}{m_{y1}} k_y^2 + \frac{m_{x1}}{m_{z1}} k_z^2). \qquad (9)$$

Here the anisotropy of effective mass was taken into account, and the dimensionless components of the size-quantized wave vector k_x, k_y, k_z are the solutions of the system of algebraic equations, similar to (8).

Let a_x, a_y, a_z are the sizes of the dot in the x, y, and z directions, and m_{i1} and m_{i2} are the components of effective masses in the direction $i = x, y, z$ inside and outside of the dot respectively.

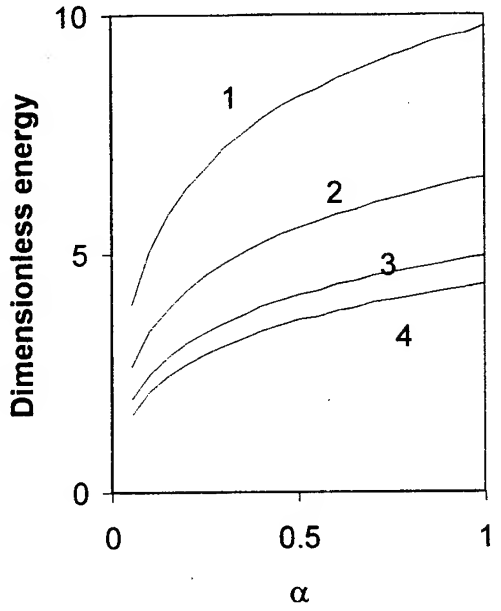

Fig.4 Dimensionless energy, $\varepsilon = \frac{2m_{x1}a_x^2 E}{\hbar^2}$, versus parameter α for χ=10, lines: 1 - $a_y / a_x = a_z / a_x = 1$; lines 2,3,4 – $a_y / a_x = a_z / a_x = 2,4,10$.

For the isotropic, but space-dependent effective mass the position of energy level strongly depends on the ratio $\alpha = m_{x1} / m_{x2}$. Fig. 4 shows the energy spectrum for the lowest level for $\chi = \frac{2m_{x1}U_0 a_x^2}{\hbar^2} = 10$. Curve 1 is for the cubic dot ($a_y / a_x = a_z / a_x = 1$), curves 2, 3, and 4 correspond to the rectangular dots with $a_y / a_x = a_z / a_x = 2,4,10$, respectively. With an increase in α, the energy level moves closer to the top of the potential dot.

Let us now consider the anisotropic effective mass in the dot $m_{x1} = m_{y1} < m_{z1}$, but isotropic effective mass in the barrier region $m_{x2} = m_{y2} = m_{z2}$, and α=1. Fig.5 shows the dependence of the energy level on the ratio m_{x1} / m_{z1} for χ=10, (curve 1) for a cubic dot and for rectangular dots $a_y / a_x = a_z / a_x = 2,4$ (curves 2 and 3). As can be seen from the figure, a decrease in anisotropy (i.e. an increase in m_{x1} / m_{z1}) leads to the bottom level moving closer to the top of the potential well. However, the effect is not too strong, and, hence, the isotropic model might serve as reasonable approximation for the calculations of the energy levels in quantum dot.

In the opposite limiting case, the effective mass is anisotropic in the barrier region $m_{x2} = m_{y2} < m_{z2}$, and isotropic in the dot region and α=1. Fig.6 shows the dependence of the enegry level on the anisotropy in the barrier region for χ=10, for cubic and rectangular dots. As can be seen from the figure, a decrease in anisotropy leads to the bottom level moving closer to the top of the potential well. However, once again, the

effect is not too strong, which confirms our conclusion that an isotropic model might serve as a reasonable approximation for the calculations of the energy levels in a quantum dot.

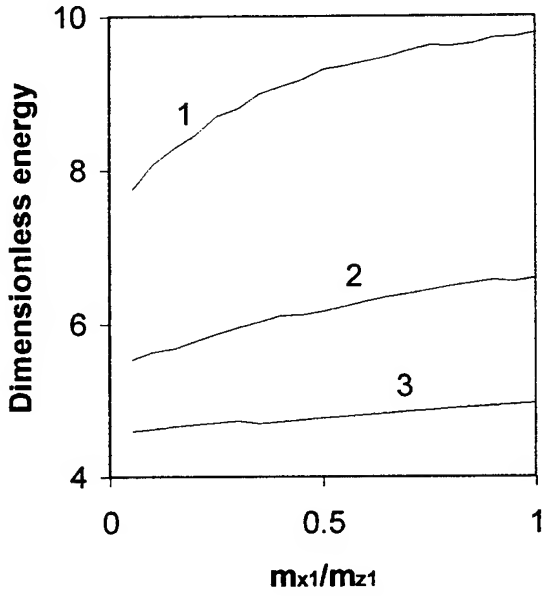

Fig.5 Dimensionless energy, ε, versus ratio m_{x1}/m_{z1} for χ=10, α=1, lines: 1 - $a_y/a_x = a_z/a_x = 1$; lines 2,3- $a_y/a_x = a_z/a_x = 2{,}4$.

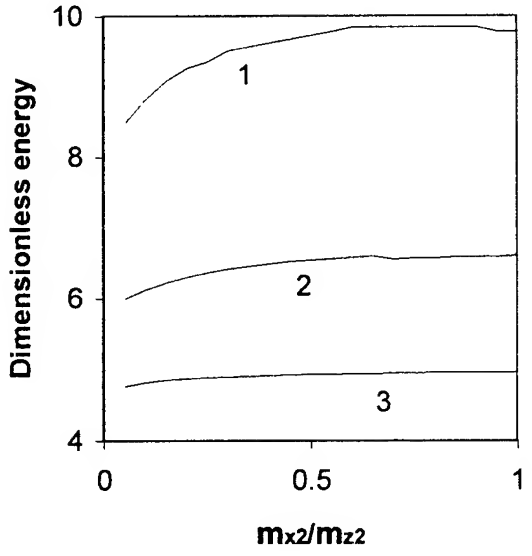

Fig. 6. Dimensionless energy, ε, versus ratio m_{x2}/m_{z2} for χ=10, α=1, lines: 1 - $a_y/a_x = a_z/a_x = 1$; lines 2, 3 - $a_y/a_x = a_z/a_x = 2{,}4$.

Conclusions

1. We considered the consequences of the space-dependence of the electron and hole effective mass on the spectra of quantum wires. Just like for quantum wells, the space dependence of effective mass leads to the appearance of additional momentum-dependent potential . As an example, the influence of anisotropy of effective mass electrons and holes was considered for Si-Ge quantum wires [9].

2. The consequences of the space-dependence of the electron (hole) effective mass on the spectra of quantum dots were considered. The space dependence of the effective mass doesn't lead to the change of the critical potential depth of the appearing of energy level in the dot. However, this dependence affects the position of the energy levels. The anisotropic effective mass has been considered [10].

3. Quantum Dot M-I-S Structures

We fabricated a M-I-S structure on the test i-Si epilayer on n^+-type substrate supplied by Professor Lagally's group. After chemical cleaning, we used photolithography to define the contacts and deposited the contact metal layer (1000Å-thick Au/800Å-thick Ag/500 Å-thick Au) by an e-beam evaporator. Current-voltage and capacitance-voltage characteristics were measured in the different parts of the wafer. A typical current-voltage characteristic of this structure is shown on the Fig.7.

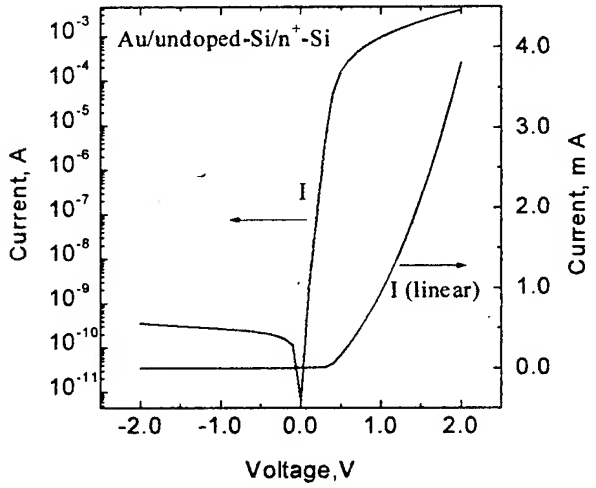

Figure 7. Current voltage characteristic of test MIS structure.

REFERENCES

1. V. Milanovich and D. Tjapkin Physica B, **114,** 375 (1982).
2. Z. S. Gribnikov , K. Hess and G. A. Kosinovsky, J. Appl. Phys . **77,** 1337 (1995).
3. M. Dyakonov and M. S. Shur , J. Appl. Phys. **84** , 3726 (1998).

4. Ogawa M, Kunimasa T, Ito T, Miyoshi T. Finite-element analysis of quantum wires with arbitrary cross sections. J Appl Phys 1998; 84(6):3242-9
5. Kenichi Nishi at al., J .Appl. Phys., **76** , 7437 (1994).
6. Min Yang, J.C. Sturm, J. Prevost , Phys. Rev. B, **56** , 1973 (1997)
7. B. Lee and K.-Y. Kim , J. Appl. Phys., **84**, 5593 (1998).
8. Landau LD. Quantum mechanics, non-relativistic theory. Oxford, Pergamon Press; 1965.
9. Borovitskaya, E.; Shur, M.S. Solid-State Electronics, **44**, no.7 p. 1293-6 (2000).
10. Borovitskaya, E.; Shur, M.S. Consequences of space dependence of effective mass in quantum dots. Accepted for publication in Solid State Electronics (2000)

4. Publications supported by the contract

E. Borovitskaya and M. S. Shur, Consequences of space dependence of effective mass in quantum wires, Solid State Electronics, Vol. 44, pp. 1293-1296 (2000)

E. Borovitskaya and M. S. Shur, Consequences of space dependence of effective mass in quantum dots, Solid State Electronics, (2000), accepted for publication

E. Borovitskaya and M. S. Shur, Editors, Quantum Dots, World Scientific, Ltd. , Singapore, in preparation